www.czasopisma.pan.pl PAN POLSKA AKADEMIA NAUK www.journals.pan.pl

Arch. Metall. Mater. **70** (2025), 4, 1619-1626

DOI: https://doi.org/10.24425/amm.2025.156241

K. WÓJCIAK[1], T. TOKARSKI[1*], G. CIOS[1], A. WINKELMANN[1], R. CHULIST[2], G. NOLZE[3,4]

UNCONVENTIONAL APPLICATIONS OF ELECTRON BACKSCATTERING DIFFRACTION (EBSD) IN METALLIC MATERIALS

Electron backscattered diffraction is widely used for phase and orientation imaging of crystalline specimens. Despite the inherent complexity of diffraction images, current analysis methodologies typically focus on the position of Kikuchi bands or direct comparisons between experimental and simulated patterns. These approaches require prior knowledge of the phases to be analyzed, limiting their applicability in certain scenarios. This paper introduces an alternative methodology, crystallographic analysis of lattice metric, which extracts phase and orientation information directly from the registered diffraction pattern without requiring predefined standards. The paper outlines the methodology, discusses limitations, and demonstrates possible application in phase analysis, lattice parameter ratio mapping, and qualitative lattice distortion mapping.

Keywords: Electron Backscatter Diffraction; Kikuchi patterns; virtual dark-field imaging; lattice distortions

1. Introduction

Electron Backscatter Diffraction (EBSD) is a fundamental and widely used technique in scanning electron microscopy for analyzing the microstructure of materials. It enables the investigation of local crystallography in crystalline and quasicrystalline materials down to the nanoscale level. An EBSD system typically comprises hardware for capturing diffracted electrons from the sample and software for processing the acquired images. Recent advancements have significantly enhanced the sensitivity of EBSD hardware, enabling applications at lower currents and voltages and achieving acquisition speeds over 5000 patterns per second [1]. The typical physical spatial resolution of EBSD ranges from 50 nm for high atomic number materials to approximately 100 nm for lighter elements [2]. Crucially, the sample's position relative to the detector geometry plays a pivotal role in determining the ultimate spatial resolution [3]. Standard EBSD acquisition is performed with the sample tilted at an angle of 70° toward the detector screen. This inclination represents a tradeoff between optimal spatial resolution and sufficient signal intensity and has become the conventional standard for EBSD measurements. The spatial resolution is inherently limited by the interaction volume of electrons within the sample [4]. During scanning, the electron beam probe the sample in predefined steps, which determine the magnification and resolution of the resulting maps. Setting step sizes below the interaction volume offers no additional structural information. Recent studies have shown that alternative tilt configurations, such as a "no-tilt" geometry, can improve spatial resolution and enable distortion-free imaging. However, these approach is relatively new, require more complex diffraction analysis, and is not yet widely adopted [5]. To address the spatial resolution limitations of traditional EBSD, Transmission Kikuchi Diffraction (TKD) was developed where instead of bulk sample, a Transmission Electron Microscopy (TEM) specimen is used [6-8]. The interaction volume is constrained by the sample's thickness, improving spatial resolution by an order of magnitude to approximately 5-20 nm for light and heavy element materials. This advancement extends capabilities of standard EBSD allowing for effective (fast and reliable) analysis of nano-crystalline materials, especially those with low atomic numbers [9].

After acquiring a diffraction image, specialized software is used to analyze the Kikuchi pattern, which is composed of bands geometrically linked to specific lattice planes. The analysis provides information on phase type and crystallographic orientation. The conventional approach to pattern analysis employs

[1] AGH – UNIVERSITY OF KRAKOW, ACADEMIC CENTRE FOR MATERIALS AND NANOTECHNOLOGY, AL. MICKIEWICZA 30. 30-059 KRAKOW, POLAND
[2] INSTITUTE OF METALLURGY AND MATERIALS SCIENCE, POLISH ACADEMY OF SCIENCES, 25 REYMONTA STR., 30-059 KRAKOW, POLAND
[3] FEDERAL INSTITUTE FOR MATERIALS RESEARCH AND TESTING (BAM), BERLIN, GERMANY
[4] TU BERGAKADEMIE FREIBERG, INSTITUT FÜR MINERALOGIE, FREIBERG, GERMANY

* Corresponding author: tokarski@agh.edu.pl

© 2025. The Author(s). This is an open-access article distributed under the terms of the Creative Commons Attribution License (CC-BY 4.0). The Journal license is: https://creativecommons.org/licenses/by/4.0/deed.en. This license allows others to distribute, remix, modify, and build upon the author's work, even commercially, as long as the original work is attributed to the author.

the Hough transform [10], an image analysis technique used for detecting geometric features such as lines or circles. First introduced by Paul Hough in 1962 [10] and applied to EBSD in 1992 [11], the Hough transform converts linear features in an image into peaks in Hough space. In the context of Kikuchi patterns, the detected peaks are used to reconstruct the 3D position of the lattice planes. The final step involves calculating interplanar angles, comparing them with theoretical phase data, and identifying the best match [12]. The angular resolution of the classical Hough transform in EBSD typically ranges from 0.5° to 0.7° [13]. Despite its limitations, this method remains a cornerstone of modern EBSD software, offering rapid automatic indexing by comparing experimental interplanar angles with tabulated values, enabling real-time data acquisition. This capability is particularly valuable for handling large datasets.

Advances in image processing, such as the application of Digital Image Correlation (DIC) algorithms [14], have further improved EBSD sensitivity [15], particularly for detecting subtle lattice distortions and orientations. Two primary high-precision techniques are Template Matching (Pattern Matching) [16] and High-Resolution EBSD (HR-EBSD) [17]. Both rely on DIC algorithms to compare each pattern either with simulated patterns (based on the dynamic theory of electron diffraction) or with a reference pattern from a deformation-free region. The degree of similarity between patterns is typically quantified using the normalized cross-correlation coefficient. These techniques enable EBSD to achieve unprecedented levels of accuracy in crystallographic analysis.

A significant advancement over the traditional Hough-based approach can be achieved through the implementation of dictionary-based template matching techniques [18]. This method is characterized by its exceptional precision and noise immunity, though it comes with the tradeoff of being relatively slow due to its brute-force nature. In template matching, pattern indexing is conducted by systematically comparing experimental diffraction patterns with a comprehensive set of reference patterns, often numbering in the thousands. One of the key strengths of template matching is its robustness and resilience to noise, enabling accurate results even in challenging conditions, such as environments with noisy or overlapping patterns. An additional step involves orientation optimization by iterative approach leading to the best match between experimental and simulated pattern. The precision of this method is sufficient for advanced applications like tetragonality mapping [19], where subtle distortions in crystal structures are effectively identified. Furthermore, template matching supports chirality mapping [20] by tracking faint and specific features in Kikuchi patterns. The technique can also be extended to analyze quasicrystals [21], thereby broadening its applicability to areas beyond the capabilities of standard Hough-based systems. The angular resolution achieved through template matching is high, typically around 0.1° or better [18], which meets the stringent requirements of detailed crystal orientation analysis. However, the successful implementation of this technique depends on prior knowledge of the material phases to be mapped, as well as access to specialized software for preparing master patterns. While the computational demands of template matching were historically a limiting factor, modern GPU-based algorithms have significantly accelerated processing times. Additional speed improvements can be achieved through the use of spherical harmonics algorithms [22], which optimize the pattern-matching process for greater efficiency.

Another technique that has recently garnered attention is High-Resolution EBSD (HR-EBSD) [17]. The term "high resolution" in this context refers to improved angular resolution allowing for lattice distortion mapping, rather than spatial resolution [15]. HR-EBSD involves comparing high-resolution diffraction images of the analyzed region with a reference pattern, which is typically obtained from a strain-free area [23]. This approach allows for precise identification of local changes in the material's microstructure [24-26], as deformation introduces subtle shifts in the positions of Kikuchi bands within the diffraction patterns. To analyze shifts, the diffraction image is divided into smaller Regions Of Interest (ROIs) [23]. The cross-correlation technique is then used to compare the ROIs from the analyzed pattern with those from the reference pattern. The resulting data can be expressed as displacement gradient components, from which strain values are calculated. Unlike conventional EBSD, HR-EBSD does not require prior orientation or phase solutions, as strain calculations are performed directly from the diffraction images. However, to couple strain data with crystallographic information, structural data must be provided, and orientations are typically resolved using methods such as the Hough transform. The sensitivity of HR-EBSD depends entirely on the accuracy of image comparison. To obtain absolute strain values, a strain-free reference pattern must be available within the dataset. A key limitation of the technique is the identification and selection of an appropriate strain-free reference image [27]. Additionally, HR-EBSD requires high-resolution, low-noise diffraction patterns (typically 1000×1000 pixels or better), which increases data acquisition times and imposes significant demands on data storage.

2. Unconventional EBSD – standard-less approach to analysis

All the aforementioned EBSD analytical methods rely on predefined crystal structures, which are fitted to diffraction patterns during analysis (with the exception of HR-EBSD, assuming only strains are calculated). A key limitation of this approach is the requirement for prior knowledge of the structure prototypes, including potential lattice variants in cases of deformation, such as during tetragonality mapping.

An alternative approach for Kikuchi diffraction analysis is offered by the CALM (Crystallographic Analysis of the Lattice Metric) algorithm [28-31], which enables the extraction of crystallographic lattice parameters directly from the diffraction pattern, provided the Projection Center (PC) is known (the origin of the diffraction signal within the sample) [23,32]. A similar approach for standard-less analysis was first proposed by Han [33], who developed an algorithm to calculate lattice

type and parameters by fitting theoretical solutions to manually traced band centers from the Kikuchi pattern. In contrast to Han's method, the CALM algorithm reconstructs the crystal lattice by leveraging the translational symmetry of the lattice. This symmetry imposes well defined relationships between diffraction planes that form the Kikuchi bands in the diffraction image [34]. The CALM algorithm has been implemented and validated in the CALM software [35].

The crystal lattice reconstruction process begins with the manual identification of four initial plane traces on the gnomonic projection of the experimental pattern (Fig. 1a). Additional traces are added by connecting intersections of existing traces. This process creates a rigid framework of mutually intersecting traces, where the positions of all subsequent traces are defined by the initial four (Fig. 1b). The traces are recalculated into 3D unit vectors, each corresponding to a unique crystallographic plane. The final step involves extracting lattice spacing information for each plane, under the constraint of translational symmetry [34]. Here, knowledge of a single lattice spacing is sufficient to deduce all others. The reconstructed spatial positions and spacings of crystallographic planes are then used to calculate reciprocal lattice vectors (Fig. 1d). From a low noise diffraction pattern, it is possible to reconstruct up to ~150 reciprocal vectors. A notable feature of the CALM software is its extensive use of the Funk transformation [36], a variation of the Radon transform applied to the stereographic projection of the diffraction pattern. This transformation enhances the visibility of weak Kikuchi bands, producing distinctive «eye-like» features in Funk space, which are further clarified using derivative-based contrast enhancement (Fig. 1c). The large number of reciprocal vectors is reduced to the Niggli cell [37] from which Bravais lattice is determined and reconstructed.

The CALM algorithm provides the lattice metric, which includes unit cell lengths a, b, c, and unit cell angles α, β, and γ. Current results indicate that, depending on the average atomic mass of the sample, the error in determining absolute lattice parameter values is approximately 4%. The error can be reduced to ~1% with additional knowledge about the average atomic number of the analyzed phase [29]. The accuracy of lattice parameter determination depends on the precise detection of Kikuchi band edges. An intensity profile of a Kikuchi band is shown in Fig. 2 by a grey curve. Band edges are character-

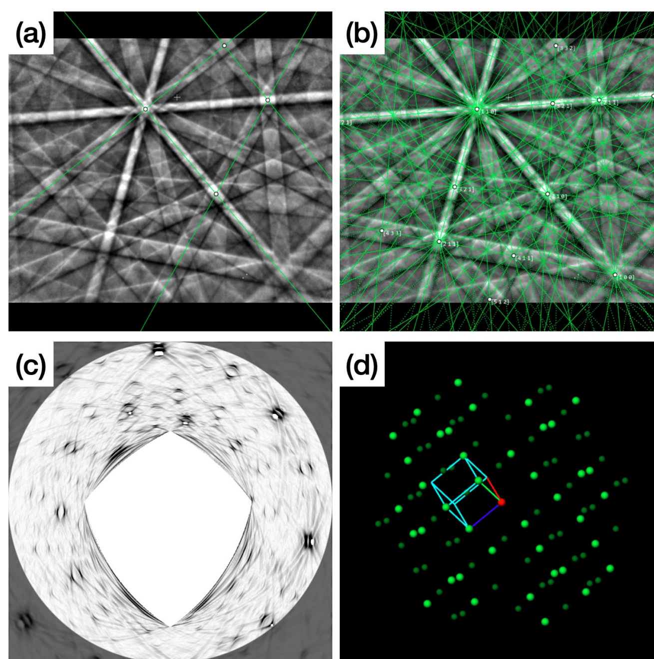

Fig. 1. Selected steps in the analysis: (a) experimental pattern with four initial trace lines marked in green, (b) fully solved experimental pattern with overlaid plane traces, (c) Funk transformation of the experimental pattern, (d) 3D representation of the reciprocal point cloud for the experimental pattern with the overlaid unit cell

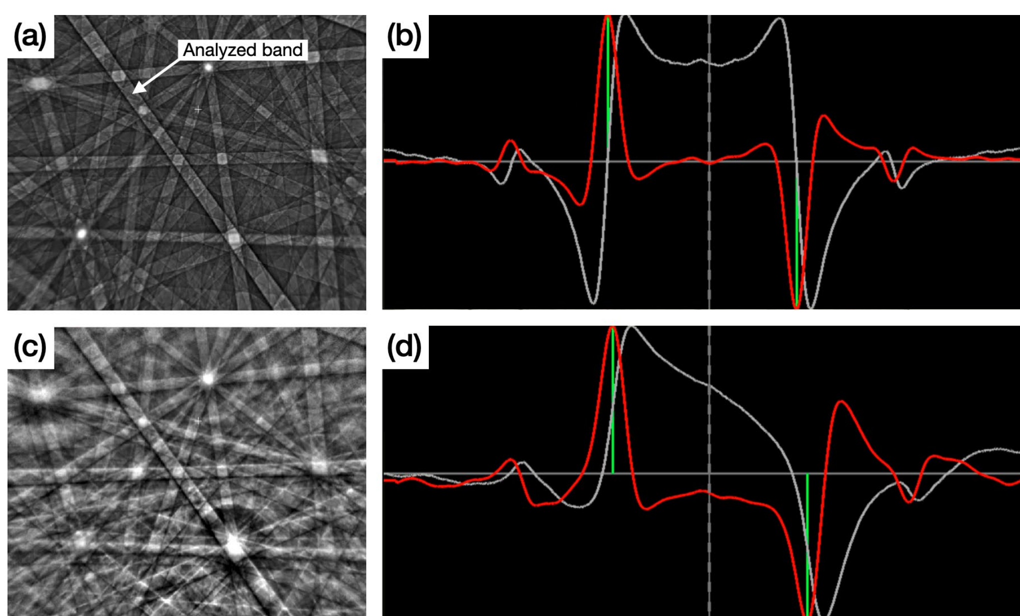

Fig. 2. Example of band profile analysis: (a) dynamical simulation of the Al_2O_3 pattern with an orientation matching the experimental pattern, (b) band profile (gray) and its first derivative (red) extracted from the simulated pattern, (c) experimental pattern of Al_2O_3 (d) the band profile (gray) and its first derivative (red) were extracted from the experimental pattern, with green vertical lines indicating the derivative extrema

ized by a gradual drop in intensity near the theoretical Bragg angle [28,29], which makes impossible accurate Bragg angle determination. In CALM, the band edge is approximated as the point of maximum slope inclination, corresponding to the peak center in the derivative of the intensity profile (red curve) [38]. Experimental challenges, such as asymmetry in band profiles caused by excess-deficiency (ED) effects or noise, further affect the accuracy of band edge detection. While simulated patterns exhibit symmetric profiles (Fig. 2a,b), experimental patterns often show significant deviations due to ED effects (Fig. 2c,d), leading to decreased accuracy in absolute lattice parameter calculations. Despite these limitations, accuracy of 0.1% is routinely achieved for good quality, low noise patterns. Contrary to absolute lattice parameters a, b and c, lattice parameters ratios c/a and b/a depend only on the spatial positions of crystal planes, as determined by trace positions on the gnomonic projection. Since trace centers are positioned midway between the left and right band edges, errors in Bragg angle estimation do not affect the calculation of lattice parameters ratios. For simulated patterns, due to the absence of ED effects and uneven backgrounds or noise, the error in calculations is at the 0.01% level. This value represents the theoretical accuracy limit of the CALM algorithm.

3. Applications of CALM algorithm

3.1. Standard-less analysis of phases

To ensure accurate results using the CALM algorithm, obtaining high-quality Kikuchi diffraction patterns is crucial. A primary consideration is minimizing noise, which can be achieved through extended exposure times or averaging multiple frames. Unlike the HR-EBSD methodology, CALM does not require high-resolution images; a resolution of approximately 300×200 pixels is adequate for analysis. An example of phase determination in the Al-Mg system is shown in Fig. 3. The analysis was performed on the Al-50 wt.% Mg master alloy cast into a steel crucible. The sample was mechanically ground using progressively finer grit SiC paper (up to 2000 mesh) and polished with 9 µm and 3 µm diamond suspensions, followed by final polishing using Struers' SiO_2 suspension (OPS). An image of the microstructure, acquired using the forward scatter detectors of an EBSD camera, is presented in Fig. 3a. The red point indicates the location where diffraction data was acquired. A high-quality diffraction pattern with a resolution of 622×512 pixels was captured using an accelerating voltage of 15 kV and a beam current of 8 nA, utilizing FEI Versa 3D scanning electron microscope and the Oxford Symmetry S2 EBSD camera (Fig. 3b). To further reduce noise, 10 frames were averaged, and both dynamic and static background compensation techniques were applied. The solution, displayed as overlaid traces in Fig. 3c, successfully reconstructed 62 Kikuchi bands, yielding a final lattice with parameters a = 10.113 Å, b = 10.117 Å, c = 10.131 Å and angles α = 76.44°, β = 76.37° and γ = 76.29°. The solution corresponds to a rhombohedral lattice with parameters a = 10.120 Å and angle α = 76.4°. Assuming the phase belongs to the Al-Mg binary system, it was matched to the $Al_{30}Mg_{23}$ phase characterized by a = 10.3625 Å and angle α = 76.4622° [39]. The errors in lattice parameter determination, when compared to literature values, are 2.6% for unit cell lengths and 0.25% for unit cell angles. The solution was additionally confirmed using the pattern matching technique. Master patterns were prepared for all phases and analyzed using the normalized cross-correlation method. The best match was obtained for the $Al_{30}Mg_{23}$ phase, where the cross-correlation coefficient was 0.732. The simulated best-fit image of the pattern is presented in Fig. 3d. It is also important to note that presented analysis provides only the lattice metrics and does not offer any information about the phase structure.

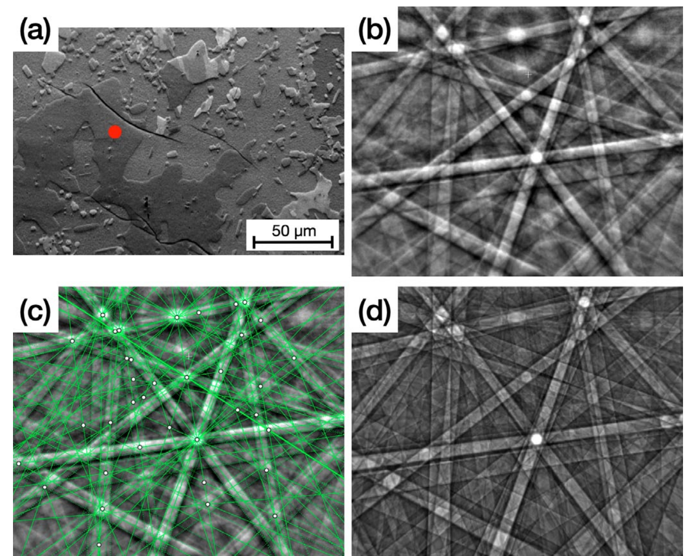

Fig. 3. Example of phase analysis: (a) microstructure image of the Al-Mg master alloy captured using a forward-scatter detector, (b) experimental diffraction pattern acquired in the spot marked by the red dot in microstructure image, (c) CALM solution corresponding to the rhombohedral Bravais lattice of the $Al_{30}Mg_{23}$ phase, and (d) dynamic simulation of the $Al_{30}Mg_{23}$ phase matching the experimental pattern

3.2. Mapping changes of lattice parameters ratios

Although CALM algorithm was originally devised for the single pattern analysis, simple automation can be used to track changes in lattice parameters within EBSD map. The analysis involves an additional step, where a rough framework of the trace intersections is prepared manually for the first pattern, and subsequent solutions of the lattice metric follows optimization routine of shifting traces to the corresponding band centres position. Utilizing fundamental feature of the CALM algorithm, which is standard-less analysis, lattice metric is reconstructed for each pattern and local changes in the lattice can be mapped with the error better than 0.1% in lattice ratios. An example of lattice parameter ratio mapping is presented in Fig. 4, showing the interface between the austenite and 10M martensite regions in a Ni-Mn-Ga alloy. The sample for analysis was prepared using standard mechanical grinding methodology with progressively

finer grit silicon carbide paper, followed by electropolishing in a solution containing 10% vol. perchloric acid in ethanol. The map was registered using FEI Versa 3D scanning electron microscope and Oxford Symmetry S2 camera operating with the following conditions: 20 kV of accelerating voltage, high beam current of ~16 nA, camera speed 25 patterns per second, pattern resolution of 622x512 pixels and map step 50 nm. The map was acquired within martensite-austenite region, where interface is localized in the right bottom part of the image (Fig. 4a). For the naked eye, differences between austenite (Fig. 4b) and martensite (Fig. 4c) patterns are almost invisible, apart from faint lines belonging to the modulations in the martensite pattern (marked by red dashed line). The variances between both patterns can be visualized using the difference image, where one zone (marked with red arrow) vanishes, while rest of the image is showing clear differences (Fig. 4d) suggesting that pattern is stretched but not rotated. The observed differences correspond to changes in the lattice parameters between austenite and martensite. The results of lattice parameters ratio $c/a = 0.950$ and $b/a = 0.993$ shows high algorithm sensitivity, where the orthorhombic unit cell of martensite can be mapped with the precision better than 0.1%.

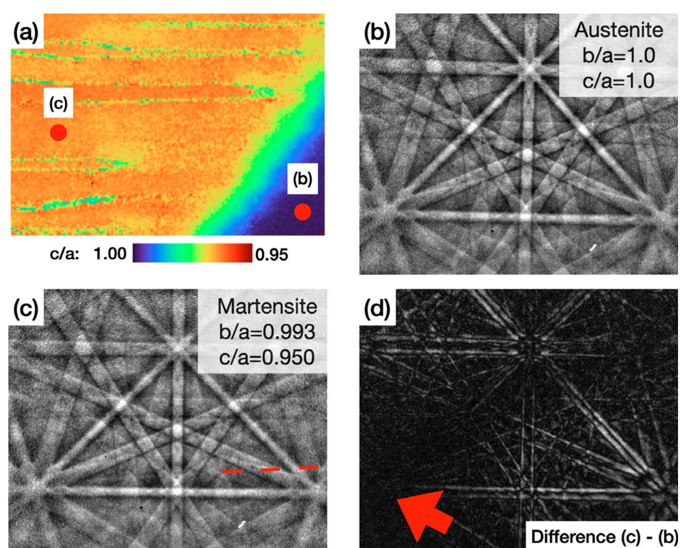

Fig. 4. Analysis of lattice parameter ratios at the interface between austenite and martensite in a Ni-Mn-Ga alloy: (a) map of the c/a parameter ratio, (b) experimental pattern from the austenite region, (c) experimental pattern from the martensite region, (d) difference image between the austenite and martensite patterns. The red arrow indicates the zone common to both patterns

3.3. Qualitative mapping of lattice deformation – dislocation imaging

Band profile analysis provides more than just information for optimizing trace positions or approximating Bragg angles; it also offers quantitative insights into the intensity and sharpness of individual Kikuchi bands. A perfect crystal with undistorted lattice planes produces a strong diffraction signal, whereas any defects introduced into the crystal lattice cause distortions that degrade the diffraction signal. This phenomenon is well known, particularly in cases where plastic deformation is applied to samples, leading to deterioration in pattern quality, often characterized by Image Quality (IQ). IQ is primarily used to qualitatively identify grain boundaries and heavily deformed regions within a sample. Detecting dislocations, however, is more challenging as it requires both high spatial resolution and high sensitivity to variations in Kikuchi band sharpness. These challenges can

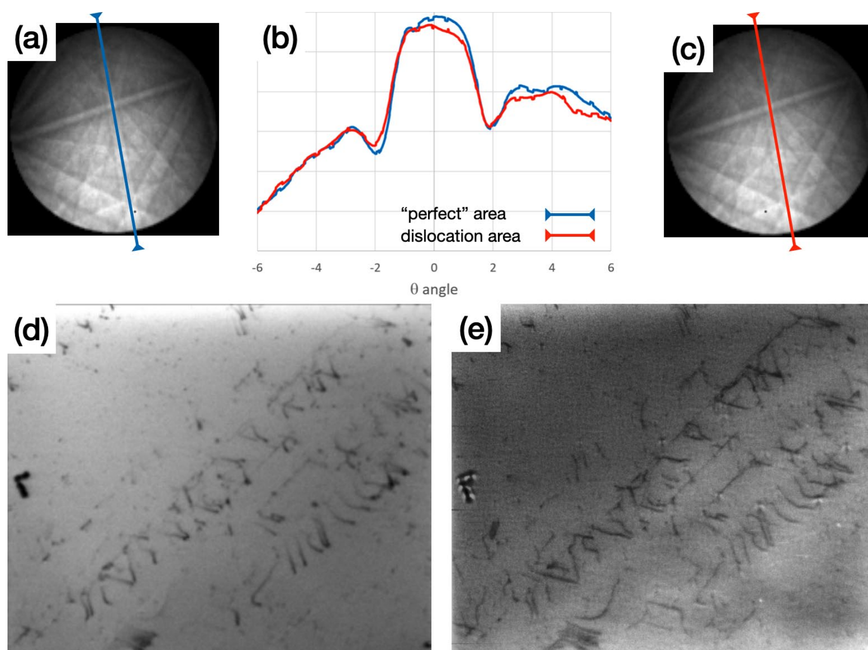

Fig. 5. Example of dislocation analysis performed in TKD mode on a thin aluminum foil: (a) pattern recorded in the undeformed region, (b) band profiles of the {022} Kikuchi band, (c) pattern recorded in the dislocation region, (d) image reconstructed from the sharpness analysis of Kikuchi band profiles, (e) image captured by the forward scatter detector

be addressed using Transmission Kikuchi Diffraction (TKD) and band profile analysis. TKD minimizes the electron-matter interaction volume, focusing on the strain distribution around dislocation cores, where strain intensities are sufficient to distinguish dislocation regions from perfect crystal regions.

An example of dislocation imaging is shown in Fig. 5. The analysis was performed on a thin foil prepared from a slightly deformed copper sample. The preparation process included mechanical thinning of the specimen to a thickness of approximately 50 µm, followed by cutting standard 3 mm TEM discs. The final step involved electropolishing using Struers' D2 electrolyte and the twin jet TenuPol-5 electropolishing unit. The map was acquired using FEI Versa 3D scanning electron microscope and EDAX Hikari camera under the following conditions: 30 kV accelerating voltage, high beam current of 16 nA, camera speed of 50 patterns per second, and a map step size of 5 nm. Patterns were recorded without any background compensation, and a dedicated shield to reduce re-scattered electrons was employed [8]. Additionally, low-resolution patterns (120×120 pixels) were used to enhance the signal-to-noise ratio. Exemplary patterns from both the dislocation and undeformed crystal regions are shown in Fig. 5(a, c). At first glance, these patterns appear indistinguishable. However, detailed analysis of individual band profiles, such as those from the {022} diffracting plane, reveals clear differences (Fig. 5b). The primary difference lies in the inclination of the band edges, which is smaller in the dislocation region (red curve in Fig. 5c). Band profile sharpness analysis was conducted for each pattern, and the resulting map is presented in Fig. 5d. The map highlights dislocation-like features that correspond to the same regions identified in the Forward Scattering Detector (FSD) image (Fig. 5e), confirming that the observed contrast changes are caused by dislocation-type defects.

4. Summary

The paper introduces the CALM algorithm as an alternative, standard-less approach for analyzing Kikuchi diffraction patterns in EBSD and TKD systems. Unlike conventional methodologies, which require prior knowledge of analyzed phases, CALM reconstructs crystallographic lattice parameters directly from diffraction patterns. This algorithm employs the translational symmetry of crystal lattices, ensuring precise determination of lattice type, lattice parameters, and orientation.

The CALM methodology begins by identifying initial Kikuchi band traces in the diffraction pattern and expanding them into a rigid framework of intersecting traces. Using this framework, reciprocal lattice vectors are calculated, and the lattice metric is extracted through reduction to the Niggli cell. Notably, CALM employs Funk transformation, enhancing the detection of weak Kikuchi bands and improving accuracy. Experimental results demonstrate an error of ~4% in determining absolute lattice parameters, which can be reduced to ~1% with supplemental atomic number data. Additionally, CALM achieves high precision in lattice parameter ratios, with errors below 0.1%, making it particularly effective for tracking subtle lattice distortions.

The CALM approach introduces an unconventional methodology in EBSD analysis, offering the following capabilities:

- Phase Analysis: CALM enables the identification of phases without standards, relying on the analysis of high-quality diffraction patterns only. For example, its application to an Al-Mg binary system demonstrated precise lattice parameter determination without the need for high-resolution images.
- Lattice Parameter Ratio Mapping: The algorithm effectively maps local variations in lattice parameters, as highlighted in a NiMnGa alloy study. It demonstrated exceptional sensitivity in distinguishing between martensitic and austenitic phases.
- Dislocation defect imaging: By utilizing subtle changes in Kikuchi band profiles, it is possible to map lattice distortions at the dislocation level. This demonstrates the exceptionally high resolution of TKD imaging and the sensitivity of band profile analysis.

Acknowledgment

This work was supported by Polish Nation Science Centre grant no. 2020/37/B/ST5/03669.

REFERENCES

[1] https://www.ebsd.com/ebsd-techniques/ebsd-detectors
[2] D. Chen, J. Kuo, The Effect of Atomic Mass on the Physical Spatial Resolution in EBSD. Microsc. Microanal. **19** (S5), 4-7 (2013). DOI: https://doi.org/10.1017/S143192761301221X
[3] F. J. Humphreys, Y. Huang, I. Brough, C. Harris, Electron backscatter diffraction of grain and subgrain structures – resolution considerations. J. Microsc. **195** (3), 212-216 (1999). DOI: https://doi.org/10.1046/j.1365-2818.1999.00579.x
[4] S.F. Bordín, S. Limandri, J.M. Ranalli, G. Castellano, EBSD spatial resolution for detecting sigma phase in steels. Ultramic. **171**, 177-185 (2016). DOI: https://doi.org/10.1016/j.ultramic.2016.09.010
[5] G. Cios, A. Winkelmann, G. Nolze, T. Tokarski, B.R. Jany, P. Bała, EBSD and TKD analyses using inverted contrast Kikuchi diffraction patterns and alternative measurement geometries. Ultramic. **267** (2), 2024. DOI: https://doi.org/10.1016/j.ultramic.2024.114055
[6] P. Trimby, Orientation Mapping of Nanostructured Materials Using Transmission Kikuchi Diffraction in the Scanning Electron Microscope. Ultramic. **120**, 16-24 (2012). DOI: https://doi.org/10.1016/j.ultramic.2012.06.004
[7] T. Tokarski, G. Cios, A. Kula, P. Bała, High quality transmission Kikuchi diffraction analysis of deformed alloys – Case study. Mat. Char. **121** (2016). DOI: https://doi.org/10.1016/j.matchar.2016.10.013

[8] T. Tokarski, G. Nolze, A. Winkelmann, Ł. Rychłowski, P. Bała, G. Cios, Transmission Kikuchi diffraction: The impact of the signal-to-noise ratio. Ultramic. **230** (2021).
DOI: https://doi.org/10.1016/j.ultramic.2021.113372

[9] Ch. Kuo, J. Kuo. S. Wang, Resolution of transmission electron backscatter diffraction in aluminum and silver: Effect of the atomic number. Ultramic. **193**, 126-136 (2018).
DOI: https://doi.org/10.1016/j.ultramic.2018.06.019

[10] P.V.C. Hough, B.W. Powell, A method for faster analysis of bubble chamber photographs. Nuovo Cim. **18**, 1184-1191 (1960).
DOI: https://doi.org/10.1007/bf02733175

[11] K. Kunze, S.I. Wright, B.L. Adams, D.J. Dingley, Advances in automatic EBSP single orientation measurements. Tex. Micr. **20**, 41-54 (1993). DOI: https://doi.org/10.1155/tsm.20.41

[12] S.I. Wright, B.L. Adams,. Automatic analysis of electron backscatter diffraction patterns. Metall. Trans. A **23**, 759-767 (1992).
DOI: https://doi.org/10.1007/bf02675553

[13] C. Maurice, R. Fortunier, 3d hough transform for indexing EBSD and Kossel patterns. J. Micr. **230** (3), 520-529 (2008).
DOI: https://doi.org/10.1111/j.1365-2818.2008.02045.x

[14] Q. Shi, D. Loisnard, Ch. Dan, F. Zhang, H. Zhong, H. Li, Y. Li, Z. Chen, H. Wang, S. Roux, Calibration of crystal orientation and pattern center of EBSD using integrated digital image correlation. Mat. Char. **178** (20121).
DOI: https://doi.org/10.1016/j.matchar.2021.111206

[15] A.J. Wilkinson, G. Meaden, D.J. Dingley, High-resolution elastic strain measurement from electron backscatter diffraction patterns: New levels of sensitivity. Ultramic. **106**, 307-313 (2006).
DOI: https://doi.org/10.1016/j.ultramic.2005.10.001

[16] G. Nolze, M. Jurgens, O. Jurgen, A. Winkelmann, Improving the precision of orientation measurements from technical materials via EBSD pattern matching. Acta Mat. **159**, 408-415 (2018).
DOI: https://doi.org/10.1016/j.actamat.2018.08.028

[17] A.J. Wilkinson, G. Meaden, D.J. Dingley, High resolution mapping of strains and rotations using electron backscatter diffraction. Mat. Scien. Tech. **22** (11), 1271-1278 (2006).
DOI: https://doi.org/10.1179/174328406x130966

[18] T. Friedrich, A. Bochmann, J. Dinger, S. Teichert, Application of the pattern matching approach for EBSD calibration and orientation mapping, utilising dynamical EBSP simulations. Ultramic. **184**, 44-51 (2018).
DOI: https://doi.org/10.1016/j.ultramic.2017.10.006

[19] G. Nolze, A. Winkelmann, G. Cios, T. Tokarski, Tetragonality mapping of martensite in a high-carbon steel by EBSD. Mat. Char. **175** (2021).
DOI: https://doi.org/10.1016/j.matchar.2021.111040

[20] A. Winkelmann, G. Cios, T. Tokarski, P. Bała, Y. Grin, U. Burkhardt, Assignment of chiral elemental crystal structures using Kikuchi diffraction. Mat. Char. **196** (4), 2022.
DOI: https://doi.org/10.1016/j.matchar.2022.112633

[21] G. Cios, G. Nolze, A. Winkelmann, T. Tokarski, R. Hielscher, R. Strzałka, I. Bugański, J. Wolny, P. Bała, Approximant-based orientation determination of quasicrystals using electron backscatter diffraction. Ultramic. **218** (2020).
DOI: https://doi.org/10.1016/j.ultramic.2020.113093

[22] G. Sparks, P.A. Shade, M.D. Uchic, S.R. Niezgoda, M.J. Mills, M. Obstalecki, High-precision orientation mapping from spherical harmonic transform indexing of electron backscatter diffraction patterns. Ultramic. **222** (2021).
DOI: https://doi.org/10.1016/j.ultramic.2020.113187

[23] T.B. Britton, J.L.R. Hickey, Understanding deformation with high angular resolution electron backscatter diffraction (HR-EBSD). Conf. Ser.: Mater. Sci. Eng. **304** (2018).
DOI: https://doi.org/10.1088/1757-899X/304/1/012003

[24] A. Wilkinson, G. Meaden, D.J. Dingley, Mapping strains at the nanoscale using electron back scatter diffraction. S. Micr. **45**, 285-294 (2009).
DOI: https://doi.org/10.1016/j.spmi.2008.10.046

[25] A.J. Wilkinson, G. Meaden, D.J. Dingley, High resolution mapping of strains and rotations using electron backscatter diffraction. Mater. Scien. Tech. **22**, 1271-1278 (2006).
DOI: https://doi.org/10.1179/174328406x130966

[26] J. Jiang, T.B. Britton, Angus J. Wilkinson, Accumulation of geometrically necessary dislocations near grain boundaries in deformed copper. Philosophical Magazine Letters **92** (11), 580-588 (2012).
DOI: https://doi.org/10.1080/09500839.2012.700412

[27] L.T. Hansen, B.E. Jackson, D.T. Fullwood, S.I. Wright, M.D. Graef, E.R. Homer, R.H. Wagoner, Influence of Noise-Generating Factors on Cross-Correlation Electron Backscatter Diffraction (EBSD) Measurement of Geometrically Necessary Dislocations (GNDs). Microsc. Microanal. **23** (3), 460-471 (2017).
DOI: https://doi.org/10.1017/S1431927617000204

[28] G. Nolze, T. Tokarski, Ł. Rychłowski, G. Cios, A. Winkelmann, Crystallographic analysis of the lattice metric (CALM) from single electron backscatter diffraction or transmission Kikuchi diffraction patternsJ. Appl. Crystall. **54** (3), 1012-1022 (2021).
DOI: https://doi.org/10.1107/S1600576721004210

[29] G. Nolze, T. Tokarski, Ł. Rychłowski, Use of electron backscatter diffraction patterns to determine the crystal lattice. Part 1. Where is the Bragg angle? J. Appl. Crystall. **56** (2), 349-360 (2023).
DOI: https://doi.org/10.1107/S1600576723000134

[30] G. Nolze, T. Tokarski, Ł. Rychłowski, Use of electron backscatter diffraction patterns to determine the crystal lattice. Part 2. Offset corrections. J. Appl. Crystall. **56** (2), 361-366 (2023).
DOI: https://doi.org/10.1107/S1600576723000146

[31] G. Nolze, T. Tokarski, Ł. Rychłowski, Use of electron backscatter diffraction patterns to determine the crystal lattice. Part 3. Pseudosymmetry. J. Appl. Crystall. **56** (2), 367-380 (2023).
DOI: https://doi.org/10.1107/S1600576723000845

[32] A. Winkelmann, G. Nolze, G. Cios, T. Tokarski, P. Bała, Refined Calibration Model for Improving the Orientation Precision of Electron Backscatter Diffraction Maps. Mat. **13** (12), (2020).
DOI: https://doi.org/10.3390/ma13122816

[33] L. Li, S. Ouyang, Y. Yang, M. Han, EBSDL: a computer program for determining an unknown Bravais lattice using a single electron backscatter diffraction pattern. J. Appl. Crystall. **47** (44), 1466-1468 (2014).
DOI: https://doi.org/10.1107/s160057671401382x

[34] G. Nolze, A. Winkelmann. Crystallometric and projective properties of Kikuchi diffraction patterns. J. Appl. Crystall. **50** (1), 102-119 (2017).
DOI: https://doi.org/10.1107/S1600576716017477

[35] https://www.calm-ebsd.com/

[36] P. Funk. Über eine geometrische Anwendung der Abelschen Integralgleichung. Math. Ann. **77**, 129-135 (1915).
DOI: https://doi.org/10.1007/BF01456824

[37] Y. Yang, C. Cai, J. Lin, L. Gong, Q. Yang, Accurate determination of lattice parameters based on Niggli reduced cell theory by using digitized electron diffraction micrograph. Micron **96**, 9-15 (2017).
DOI: https://doi.org/10.1016/j.micron.2016.12.006

[38] N. Saowadee, K. Agersted, J.R. Bowen, Lattice constant measurement from electron backscatter diffraction patterns. J. Microsc. **266**, 200-210 (2017).
DOI: https://doi.org/10.1111/jmi.12529

[39] H.L. Su, M. Harmelin, P. Donnadieu, C. Baetzner, H.J. Seifert, H.L. Lukas, G. Effenberg, F. Aldinger, Experimental investigation of the Mg-Al phase diagram from 47 to 63 at.% Al, J. Alloys Compd. **247**, 57-65 (1997).
DOI: https://doi.org/10.1016/S0925-8388(96)02595-9